Photoacoustic Fourier Transform Near- and Mid-Infrared Spectroscopy for Measurement of Energy Levels of Electron Trapping Sites in Titanium(IV) Oxide Photocatalyst Powders

Tatsuki Shinoda,[1] Naoya Murakami[1,2,]*

[1]Graduate School of Life Science and Systems Engineering, Kyushu Institute of Technology, 2-4 Hibikino, Wakamatsu-ku, Kitakyushu 808-0196, Japan

[2]Department of Applied Chemistry, Faculty of Engineering, Kyushu Institute of Technology, 1-1 Sensui-cho, Tobata-ku, Kitakyushu-shi, Fukuoka, 804-8550, Japan

ABSTRACT

Electron trapping sites in titanium(IV) oxide photocatalyst powders were investigated by photoacoustic (PA) Fourier transform near-infrared spectroscopy (FT-NIR), and mid-infrared spectroscopy (FT-MIR). PA measurements using FT-NIR and FT-MIR enabled *in situ* observation of the energy levels of electron trapping sites in wide energy levels (0.1-1.9 eV) below the bottom of the conduction band. During ultraviolet (UV) irradiation, PA intensity increased depending on the wavenumber, and changes in the PA spectra were observed as a

result of the trivalent titanium species generated by accumulation of electrons at trapping sites. Moreover, the PA spectral shape during UV irradiation was essentially different between the crystal structures, and it greatly depended on the crystal structure rather than other properties such as specific surface area and particle size. The results for various samples suggest that anatase has shallower energy levels of electron trapping sites than those of rutile and brookite, with the main energy level of the trapping sites being deep in the order of brookite > rutile > anatase. Thus, the PA technique using FT-NIR and FT-MIR is an effective method for measurements of energy levels of electron trapping sites in semiconductor photocatalysts.

INTRODUCTION

Titanium(IV) oxide (TiO_2), which is a representative semiconductor photocatalyst, has been widely used for the purpose of environmental purification and self-cleaning.[1,2] Photocatalytic reactions are induced by photoexcited electrons and positive holes generated by irradiation with excited light, and the activated species induce redox reactions with adsorbates on the surfaces of semiconductor materials.[1] However, the efficiency of the reaction decreases when recombination between photoexcited electrons and positive holes occurs. The trapping sites are thought to behave as recombination centers and accelerate the recombination rate, whereas it has also been reported that they promote charge separation and suppress recombination.[3] These different impacts of trapping sites on recombination are possibly due to the energy levels of trapping sites. Thus, the energy levels of electron/hole trapping sites are important for the reaction efficiency of a photocatalytic reaction.

2

Trivalent titanium (Ti^{3+}) species are considered to be representative trapping sites in TiO_2 and they have been investigated by a photochemical method using methylviologen as a redox indicator,[4] electron paramagnetic resonance,[5-7] spectroelectrochemical method[8,9] and electronic absorption spectroscopy[10-13]. Ti^{3+} species are formed by electron accumulation in titanium sites with oxygen vacancies. Furthermore, there is an almost linear relation between Ti^{3+} density (the molar amount of trapped electrons in titanium sites) and the electron-hole recombination rate constant, indicating that Ti^{3+} species reflect recombination sites.[4] It has been estimated that the energy levels of Ti^{3+} are 0-0.4 eV below the bottom of the conduction band, and it has been shown that the excitation energy from the trapping site to the bottom of the conduction band corresponds to photon energy of the mid-infrared (IR) region.[4,8,9,12] Therefore, Fourier transform mid-infrared spectroscopy (FT-MIR) has been used to analyze free electrons in the conduction band and shallowly trapped electrons.[14-21]

Transmission method,[14-16] diffuse reflection method[17,18] and attenuated total reflection method[19-21] are often used as FT-MIR methods for observation of semiconductor materials, such as TiO_2. These FT-MIR studies revealed shallow energy levels of electron trapping sites in TiO_2 and trapping processes of photogenerated electrons near the surface. However, due to the impact of adsorbed H_2O and residual organic compounds, samples must be pretreated, and FT-MIR measurements have been carried out in a high vacuum in some studies. Therefore, there is a possibility that the properties of samples under FT-MIR measurement conditions are different from those under real photocatalytic conditions.

A photoacoustic (PA) method is applied to photocatalytic conditions without any pretreatment of a sample because it enables detection of the photoabsorption of a sample as pressures change in the surrounding atmosphere gas regardless of sample form.[22,23] Actually, *in situ* observation

of Ti^{3+} in TiO_2 has carried out using a PA technique.[10-13,24-27] In a previous study, we established a photoacoustic Fourier transform infrared spectroscopy (FTIR-PAS) system using the combination of an Fourier transform infrared spectroscopy (FTIR) system with photoacoustic spectroscopy (PAS) for *in situ* observation of the photocatalytic decomposition of an organic compound over TiO_2 powder.[28] We also analyzed the energy levels of Ti^{3+} in the wavenumber range of 800 to 6000 cm^{-1} (0.1-0.7 eV) by measuring FTIR-PAS spectra using an FT-MIR spectrometer.[26] However, FTIR-PAS studies in a region of a wavenumber higher than 6000 cm^{-1} could not be performed due to the limitation of the IR source of an FT-MIR spectrometer.

In the present study, an FTIR-PAS system was developed for analysis of deeper energy levels, where a Fourier transform near-infrared spectroscopy (FT-NIR) spectrometer was used for extension of the wavenumber. FT-NIR has been used for qualitative and quantitative analyses of various kinds of products including food,[29,30] wood,[31,32] polymers[33,34] and pharmaceuticals[35]. FT-NIR techniques enable observation of chemical and physical properties such as molecular structure, density, and viscosity. These properties are attributed to changes in absorption intensity and shift of the overtones and combination modes of functional groups, e.g., X-H bonds (X = C, O, N).[36] Therefore, FT-NIR is used to study the molecular structures of complexes,[37,38] anharmonicity,[39] phase transition[33,34] and crystallization processes[40]. On the other hand, there have been no FT-NIR studies on the electronic states of semiconductor photocatalysts. The present study was performed to clarify the crystal structure dependence of energy levels of Ti^{3+} in the wavenumber range of 800 to 15000 cm^{-1} (0.1-1.9 eV). This study is the first study in which analysis of the energy levels of electron trapping sites in a semiconductor photocatalyst was conducted by using FT-NIR.

EXPERIMENTAL SECTION

Materials

Sixteen TiO_2 powders from reference catalysts supplied by the Catalyst Society of Japan (JRC-TIO series) and commercial products (TAYCA AMT series, Ishihara Sangyo ST series, Showa Titanium F-6A, TAYCA MT series, TAYCA TKP series, Ishihara Sangyo CR-EL, Merck TiO_2 powder, Kojundo Chemical Laboratory brookite TiO_2 powder) were used without any pretreatment (Table 1).

Estimation of Ti^{3+} density by PAS

For sample preparation, 200 mg of a powder sample was dispersed in an aqueous ethanol solution (10 mL, 50 vol%) by applying ultrasound treatment. The suspension (1.5 mL) was transferred to a cuvette of a PA cell and bubbled with argon gas for air removal. Details of the set-up for PAS measurements were reported previously.[24,41] A laboratory-made PA cell composed of an acrylic body and a quartz window was used. For PAS measurements, the PA cell was attached to a UV-transparent disposable cuvette with a 6 mmφ hole, which was covered with a cover glass (Matsunami Glass, 0.04-0.06 mm). A laser diode (Edmund Optics, 84-930, emission at 532 nm, 15 mW) was used as a probe light and its output intensity was modulated by a function generator (NF, DF1906) at 2.6 Hz. From the opposite side of the probe light, the sample suspension was photoexcited by UV irradiation using a light-emitting diode (Nichia NCSU033B, emission around 365 nm, 8.7 mW cm^{-2}).

The PA signal, which reflects Ti^{3+} species, was acquired by a digital MEMS microphone (STMicroelectronics Inc., STEVAL-MKI155V2) and Fourier-transformed with a Hamming window function. The time courses of generation and extinction of Ti^{3+} were observed, and data were obtained at intervals of 20 seconds (Figure S1). At that time, methylene blue was used as a redox indicator. From the consumption of methylene blue by electron-transfer reaction between Ti^{3+} and methylene blue, the Ti^{3+} density was estimated (Figure S2).

FTIR-PAS measurements

Details of the set-up for FTIR-PAS measurements were reported previously.[28] A laboratory-made PA cell consisting of a duralumin body, a sample holder, a calcium fluoride (CaF_2) window and two gas-exchange valves was used. Two types of FTIR spectrometers, which were Frontier NIR (PerkinElmer, mirror velocity: 0.1 cm s^{-1}) and Nicolet iS10 (Thermo Fisher Scientific, mirror velocity: 0.3165 cm s^{-1}), were used as probe lights. For FTIR-PAS measurements, approximately 100 mg of a sample was loaded on a sample holder and placed in the PA cell, and nitrogen gas or oxygen gas containing gaseous ethanol (N_2+EtOH, O_2+EtOH) was flowed through the gas flow passage to the PA cell and then the cell was closed tightly. The sample was photoexcited by UV irradiation using a light-emitting diode (Nichia NCSU033B, emission around 365 nm, 8.8 mW cm^{-2}).

The measurements were performed in the wavenumber range of 800 to 15000 cm^{-1} (0.1-1.9 eV) in a closed system at room temperature, and the PA signal, corresponding to absorption of the sample in the range of the near-IR (NIR) to mid-IR (MIR) region, was acquired by a digital MEMS microphone (TDK Invensense, ICS-43432) before and during UV irradiation. The

acquired PA signal (interferogram) was Fourier-transformed with a Hap-Genzel window function. Subsequently, the PA spectra were obtained by normalizing with carbon black powder (Kojundo Chemical Laboratory Co.), which can completely absorb lights of the IR source (Figure S3).

Table 1. Physical and chemical properties of TiO_2 samples

Name	Supplier	Crystal structure	Specific surface area / m^2 g^{-1}	Ti^{3+} density / μmol g^{-1} [a]
AMT-100	TAYCA	Anatase	302[f]	80
AMT-600	TAYCA	Anatase	55[f]	60
ST-01	IS[b]	Anatase	344[f]	69
ST-21	IS[b]	Anatase	67[f]	67
ST-41	IS[b]	Anatase	11[f]	7
JRC-TIO-1	CSJ[c]	A/R[e]	79[f]	63
JRC-TIO-15	CSJ[c]	A/R[e]	53[f]	57
F-6A	Showa Denko	A/R[e]	308[f]	117
TKP-101	TAYCA	Anatase	114[f]	27
TKP-102	TAYCA	Anatase	46[f]	40
MERCK	MERCK	Anatase	12[f]	3
MT-150A	TAYCA	Rutile	114[f]	87
MT-600B	TAYCA	Rutile	27[g]	10
JRC-TIO-6	CSJ[c]	Rutile	102[f]	60
CR-EL	IS[b]	Rutile	8[f]	13
Brookite	KCL[d]	Brookite	23[h]	40

[a] Ti^{3+} density was obtained by a PA technique (Ref. 24). [b] IS: Ishihara Sangyo. [c] CSJ: Catalyst Society of Japan. [d] KCL: Kojundo Chemical Laboratory. [e] Predominantly anatase phase. [f] Ref. 13. [g] Ref. 25. [h] Ref. 42.
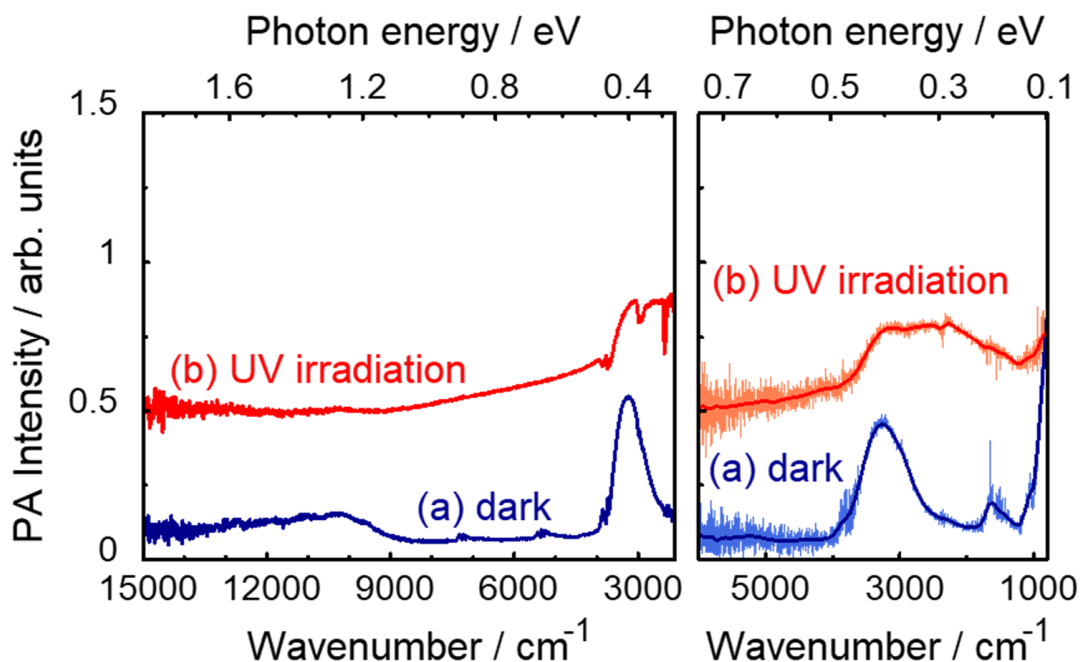
Figure 1. FTIR-PAS spectra of anatase TiO_2 powder (AMT-100) under N_2+EtOH (a) before and (b) during UV irradiation. Measurements were carried out by using FT-NIR (left) and FT-MIR (right) spectrometers.

RESULTS AND DISCUSSION

Detection of the energy levels of Ti^{3+} in anatase TiO_2 powders Figure 1a shows FTIR-PAS spectra of anatase TiO_2 powder (AMT-100) under N_2+EtOH before UV irradiation. Characteristic peaks attributed to ethanol hindering in the spectra of TiO_2 were not clearly observed because an excessive amount of ethanol vapor was removed by the flow of nitrogen gas. In the dark, broad peaks at around 10000, 7300, 5300, 3200 and 1600 cm^{-1} were observed, and they were assigned to adsorbed H_2O as in previous studies.[17,43,44] The monotonic increase in PA

intensity in the wavenumber region below 1000 cm^{-1} is due to the lattice vibration (phonon) of TiO$_2$[15,18] and/or measurement error due to low transmittance of the CaF$_2$ window of the PA cell.

Figure 1b shows FTIR-PAS spectra of anatase TiO$_2$ powder (AMT-100) under N$_2$+EtOH during UV irradiation. As in the dark condition, characteristic peaks of organic compounds were not seen. PA intensity increased during UV irradiation compared with that in the dark condition and the intensity was saturated after 30 minutes. This increase in PA intensity varied depending on the wavenumber, i.e., photon energy. In FT-NIR measurement, a broad absorption in the entire wavenumber range of 15000 to 2100 cm^{-1} was observed during UV irradiation, with the intensity increasing as the wavenumber decreased. In FT-MIR measurement, an upward shift of the FTIR-PAS spectrum was observed during UV irradiation, and the peak at 2322 cm^{-1} corresponded to 0.29 eV of photon energy.
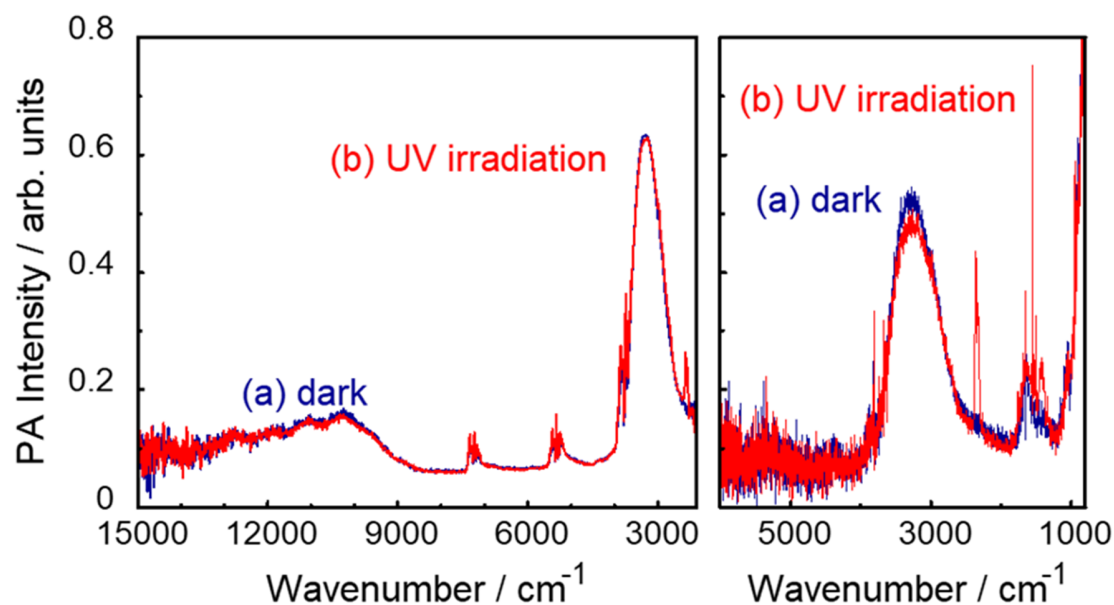
Figure 2. FTIR-PAS spectra of anatase TiO_2 powder (AMT-100) under O_2+EtOH (a) before and (b) during UV irradiation. Measurements were carried out by using FT-NIR (left) and FT-MIR (right) spectrometers.

The same experiment was carried out under O_2+EtOH. Figure 2a shows FTIR-PAS spectra of anatase TiO_2 powder (AMT-100) under O_2+EtOH before UV irradiation. In the dark, the spectral shape was similar to that under N_2+EtOH. However, the spectra under an oxygen atmosphere during UV irradiation were totally different from those under a nitrogen atmosphere (Figure 2b). A broad absorption in the wavenumber range of 15000 to 2100 cm^{-1} and an upward shift of the FTIR-PAS spectrum were not seen, whereas characteristic peaks of gaseous species and adsorbates on the TiO_2 were observed. The peaks at around 2280-2390 cm^{-1} were attributed to carbon dioxide, while sharp peaks at around 1710, 1650 and 1550 cm^{-1} were due to adsorbed acetaldehyde, acetyl and acetate, respectively.[45,46] In addition, a noise peak at around 3600-4000

cm^{-1} attributed to H$_2$O vapor was observed.[44]   Evolution of these gaseous species and intermediates seems to be due to the photocatalytic oxidation of ethanol over TiO$_2$. Thus, these results indicate that UV irradiation induced an increase in PA intensity under N$_2$+EtOH, that is, the appearance of a broad absorption and an upward shift is assigned to the formation of Ti^{3+} generated by electron accumulation. Variation of PA intensity depending on the wavenumber also reflects the energy levels and amount of Ti^{3+}. A control experiment was carried out under nitrogen gas containing pure water vapor in place of EtOH. Spectral changes during UV irradiation were observed, but the changes were much smaller than that under N$_2$+EtOH (Figure S4). This result obviously shows that ethanol as sacrificial hole scavenger is necessary for generation of Ti^{3+}. In general, it is well known that IR absorption of free electrons in the conduction band varies exponentially as a function of the wavenumber, with the absorption intensity increasing as the wavenumber decreases.[15] In contrast, IR spectra of the electrons at trapping states show a broad feature, which is due to optical transition from trapping sites into the conduction band. As shown in Figure 1b, the monotonic increase in PA intensity in the wavenumber range below 1000 cm^{-1} is attributed to an inter-band transition of free electrons into the conduction band or an optical transition of trapped electrons from shallow trapping sites into the conduction band. From a difference spectrum between before and during UV irradiation for anatase TiO$_2$ powder (AMT-100), the peak position is estimated to be 2245 cm^{-1}, which indicates that the energy levels of Ti^{3+} lie mainly at 0.28 eV of photon energy below the bottom of the conduction band (Figure S5).
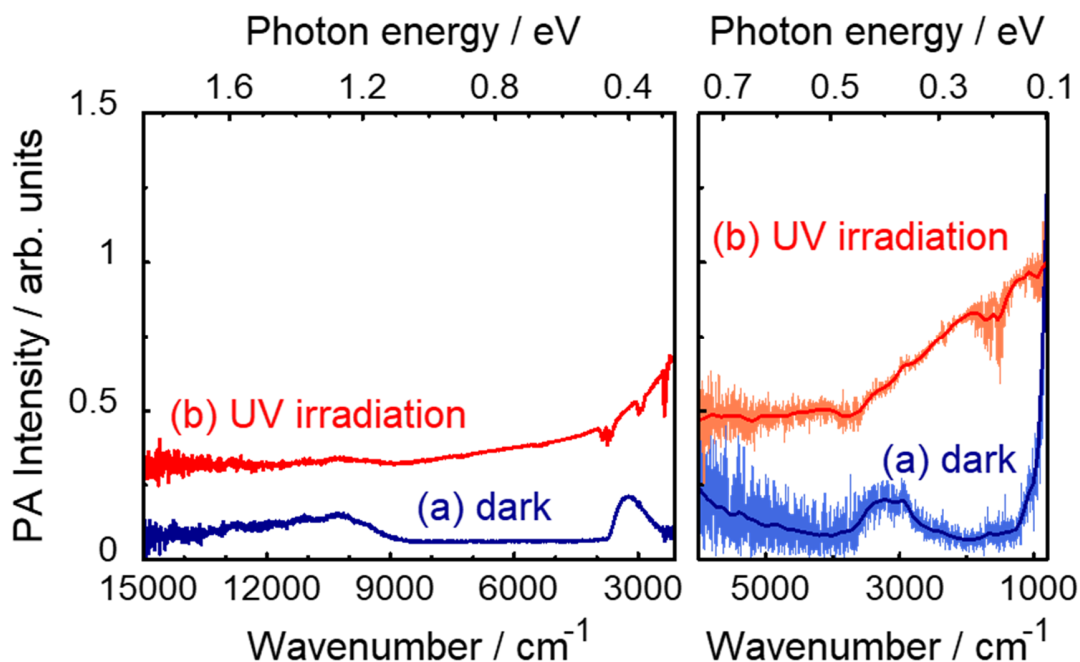
Figure 3. FTIR-PAS spectra of anatase TiO_2 powder (AMT-600) under N_2+EtOH (a) before and (b) during UV irradiation. Measurements were carried out by using FT-NIR (left) and FT-MIR (right) spectrometers.

The same experiment was also carried out under N_2+EtOH for another anatase sample. Figure 3a shows FTIR-PAS spectra of anatase TiO_2 powder (AMT-600) under N_2+EtOH before UV irradiation. The broad-absorption intensity at around 3200 cm^{-1} due to adsorbed H_2O was smaller than that of AMT-100, while broad peaks at around 7300, 5300 and 1600 cm^{-1} were not seen; however, the spectral shape was similar to that of AMT-100. During UV irradiation, PA intensity increased with irradiation time and then a broad absorption in the wavenumber range of 15000 to 2100 cm^{-1} and an upward shift of FTIR-PAS spectrum were observed. The broad-absorption intensity in the range of 15000-2100 cm^{-1} shows an upward trend with decrease in the wavenumber. The upward shift increased with a decrease in the wavenumber, and the peak at

1052 cm^{-1} corresponded to 0.13 eV of photon energy. For anatase TiO$_2$ powder (AMT-600), the peak position of a difference spectrum between before and during UV irradiation is estimated to be 1287 cm^{-1}, which indicates that the energy levels of Ti^{3+} lie mainly at 0.16 eV of photon energy below the bottom of the conduction band (Figure S6). Thus, AMT-600 possesses shallower energy levels of Ti^{3+} than those of AMT-100, though distributions of energy levels of Ti^{3+} for AMT-600 are similar to those for AMT-100.

Crystal structure dependence of the energy levels of Ti^{3+}

The energy levels of Ti^{3+} for rutile samples were also detected by measuring FTIR-PAS spectra under N$_2$+EtOH. Rutile samples showed fundamentally the same FTIR-PAS spectra in the dark as those of anatase samples, but the spectral shapes during UV irradiation were totally different from those of anatase. Figure 4 shows FTIR-PAS spectra of rutile TiO$_2$ powder (MT-150A) under N$_2$+EtOH before and during UV irradiation. A broad absorption in the wavenumber range of 15000 to 2100 cm^{-1} was observed during UV irradiation, and the peak at 7875 cm^{-1} corresponded to 0.98 eV of photon energy. An upward shift during UV irradiation was also observed for a rutile sample, with the intensity decreasing as the wavenumber decreased. For rutile TiO$_2$ powder (MT-150A), an absorption peak was not observed in the MIR region, whereas it was seen in the NIR region. The peak position of a difference spectrum between before and during UV irradiation is estimated to be 7813 cm^{-1}, which indicates that the energy levels of Ti^{3+} lie mainly at 0.97 eV of photon energy below the bottom of the conduction band (Figure S7). The spectral feature during UV irradiation disagrees with results of previous FT-MIR studies, which showed that the spectral shape of rutile was similar to that of anatase and

that the absorption intensity increased with decrease in the wavenumber.[15,16,18] Instead, the FTIR-PAS spectra resembled the transient absorption spectra of rutile TiO_2.[47] This result suggests that the energy levels of Ti^{3+} in rutile are much deeper than those in anatase, and photogenerated electrons are trapped at deep trapping sites.
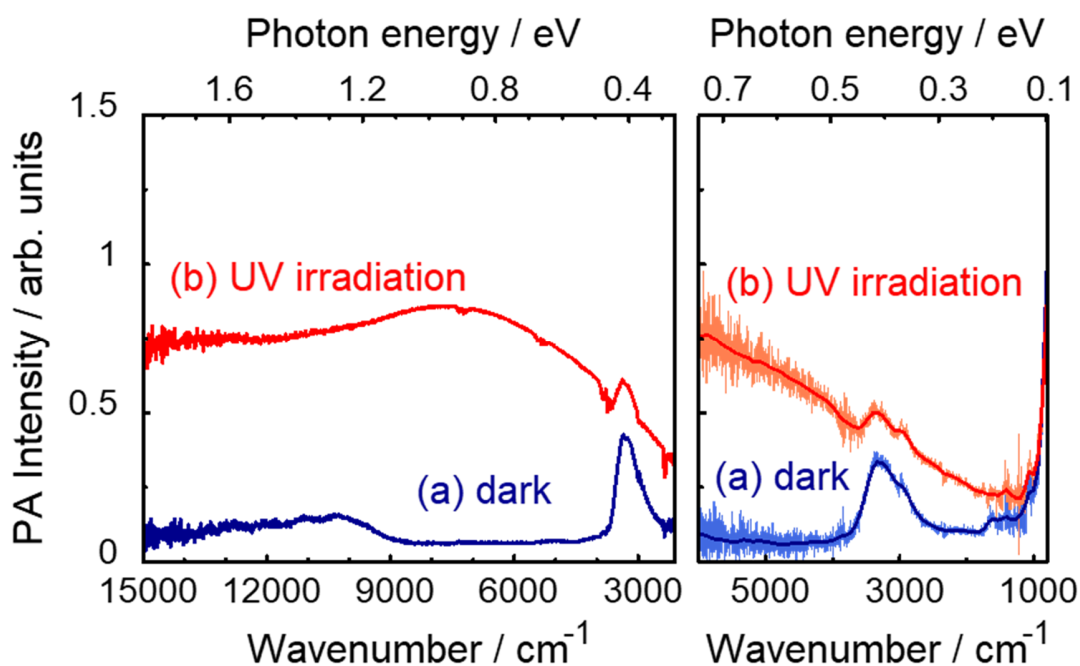

Figure 4. FTIR-PAS spectra of rutile TiO_2 powder (MT-150A) under N_2+EtOH (a) before and (b) during UV irradiation. Measurements were carried out by using FT-NIR (left) and FT-MIR (right) spectrometers.
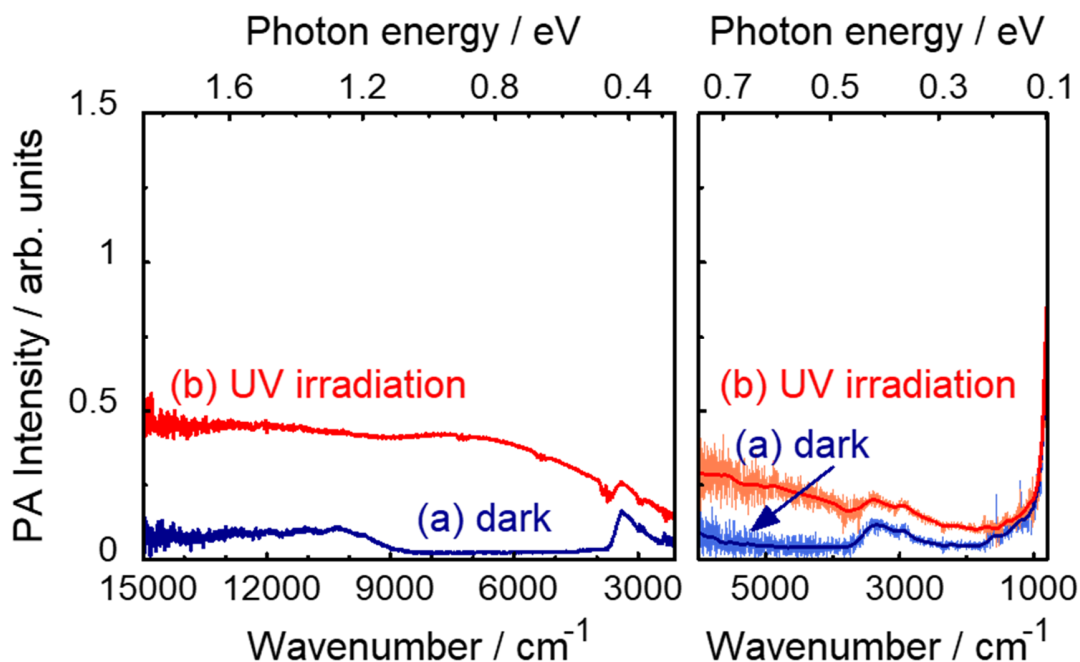
Figure 5. FTIR-PAS spectra of rutile TiO_2 powder (MT-600B) under N_2+EtOH (a) before and (b) during UV irradiation. Measurements were carried out by using FT-NIR (left) and FT-MIR (right) spectrometers.

The same experiment was also carried out for another rutile sample. Figure 5 shows FTIR-PAS spectra of rutile TiO_2 powder (MT-600B) under N_2+EtOH before and during UV irradiation. The spectral shape during UV irradiation was similar to that of MT-150A, but the intensity was clearly decreased. A broad absorption in the wavenumber range of 15000 to 2100 cm^{-1} was observed, and the peak at 8147 cm^{-1} corresponded to 1.0 eV, with the intensity increasing as the wavenumber increased. The peak position of a difference spectrum between before and during UV irradiation is estimated to be 8147 cm^{-1}, which indicates that the energy levels of Ti^{3+} lie mainly at 1.0 eV of photon energy below the bottom of the conduction band (Figure S8). This

16

result indicates that both MT-150A and MT-600B possess deep trapping sites despite having different physical properties such as specific surface area.

The same experiment was carried out for a brookite sample. Figure 6 shows FTIR-PAS spectra of brookite TiO_2 powder under N_2+EtOH before and during UV irradiation. The spectral shape for the brookite sample was similar to those for anatase and rutile in the dark, but the spectral shape during UV irradiation was different from those of anatase and rutile. In the MIR region, an upward shift during UV irradiation was almost constant regardless of the wavenumber. On the other hand, PA intensity increased with increase in the wavenumber in the NIR region, and the broad absorption was similar to that of rutile such as MT-600B (Figure 5). Furthermore, it also has a resemblance to transient absorption spectra of brookite TiO_2.[42] The peak position of the difference spectrum between before and during UV irradiation is estimated to be 8631 cm^{-1}, which indicates that energy levels of Ti^{3+} lie mainly at 1.1 eV of photon energy below the bottom of the conduction band (Figure S9). Thus, brookite is thought to possess deep trapping sites in comparison with those of anatase and rutile.

The energy levels of Ti^{3+} in other samples of anatase or rutile were also investigated by observing FTIR-PAS spectra under N_2+EtOH. The spectral shape during UV irradiation mainly depended on the crystal structure rather than other properties such as specific surface area. The energy levels of Ti^{3+} for 16 samples of anatase, rutile and brookite were below the bottom of the conduction band in the ranges of about 0.11-0.28, 0.94-1.0 and 1.1 eV, respectively. These results indicate that the energy level of Ti^{3+} is greatly dependent on the crystal structure and that electron trapping sites are deep in the order of brookite > rutile > anatase. It is reported that the energy levels of electron trapping sites in rutile are much deeper than those in anatase,[48,49] and

they are estimated to be about 0.2 and 1 eV below the bottom of the conduction band for anatase

and rutile, respectively[49]. These studies give support to our experimental results.
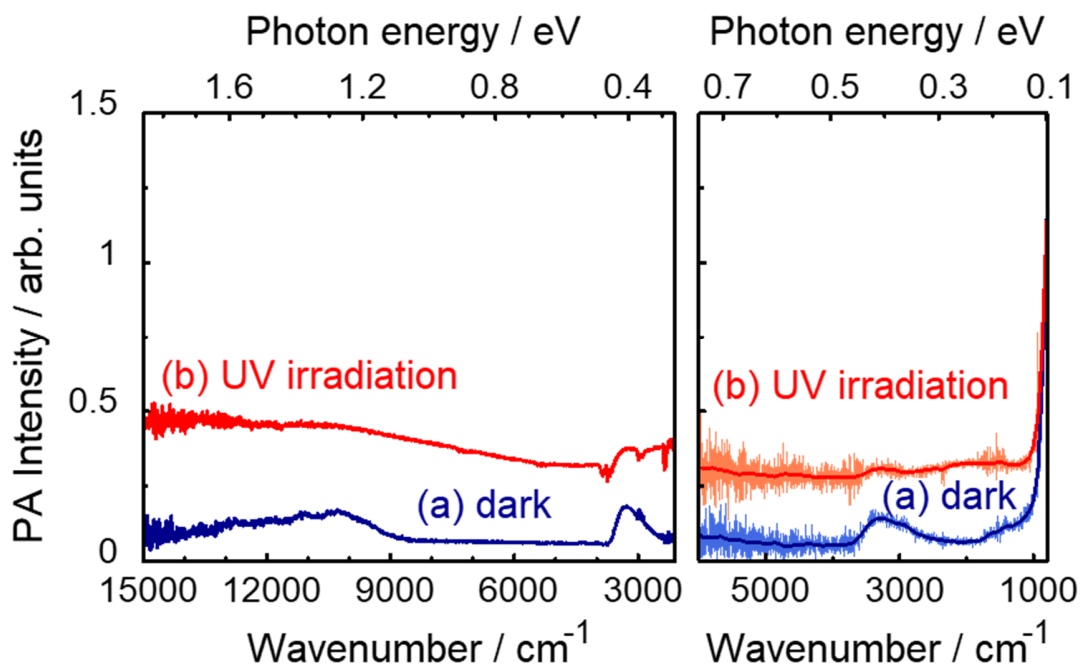

Figure 6. FTIR-PAS spectra of brookite TiO_2 powder under N_2+EtOH (a) before and (b) during

UV irradiation. Measurements were carried out by using FT-NIR (left) and FT-MIR (right)
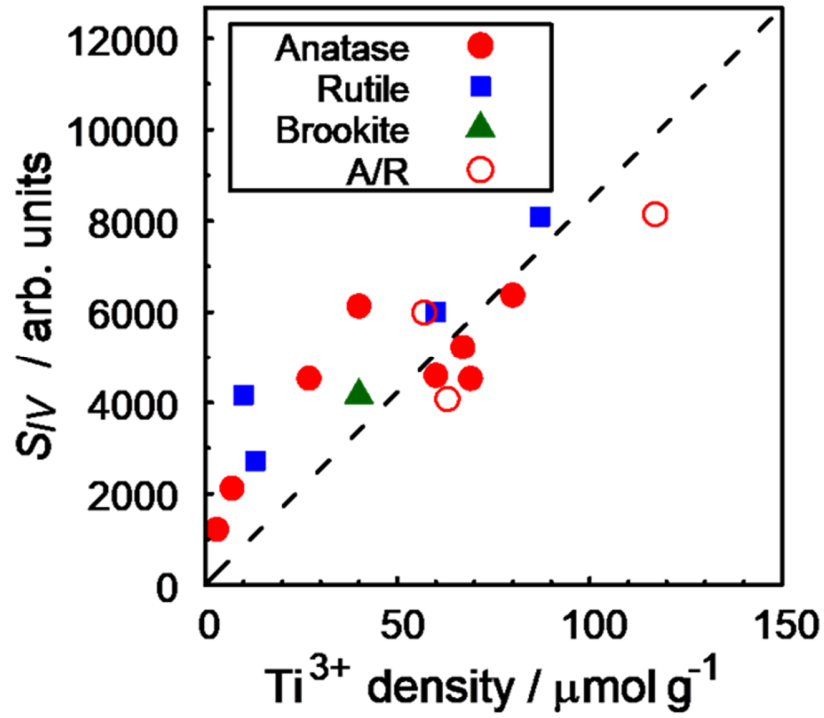
spectrometers.

Figure 7. Relation between S_{IV} and Ti^{3+} density. Filled circles, filled squares, filled triangle and open circles denote anatase, rutile, brookite and a mixture of anatase and rutile (A/R, predominantly anatase), respectively.

Comparison with Ti^{3+} density Spectral changes under an insert gas atmosphere in the presence of electron donors are thought to be due to Ti^{3+} generated by electron accumulation. Moreover, since the increment of PA intensity by UV irradiation corresponds to the amount of Ti^{3+}, the integral value (S_{IV}) was calculated as follows.

(1) In the FT-MIR measurements, the difference spectra before and during UV irradiation in the wavenumber range of 800 to 3000 cm^{-1} were integrated.

(2) In the FT-NIR measurements, the difference spectra in the wavenumber range of 3000 to 15000 cm^{-1} were integrated.

(3) The sum of (1) and (2) integral values is S_{IV}.

Figure 7 shows relation of S_{IV} of various TiO_2 samples with Ti^{3+} density measured via the time course of PAS measurement using methylene blue as a redox indicator.[24] S_{IV} and Ti^{3+} density have an almost linear relation regardless of the crystal structure, indicating that the increment of PA intensity is attributed to the amount of Ti^{3+}, i.e., electrons at trapping sites. However, compared with the extrapolation line obtained by the linear relation between S_{IV} and Ti^{3+} density, S_{IV} of many samples against Ti^{3+} density was larger. The reason for this is that Ti^{3+} density was estimated by photoexcitation of only Ti^{3+} at a certain energy level due to monochromatic irradiation (532 nm), while S_{IV} in the present study reflects photoexcitation of Ti^{3+} at various energy levels (0.1-1.9 eV).

CONCLUSIONS

An FTIR-PAS system to analyze of the energy levels of electron trapping sites in TiO_2 powders has been developed. An FT-NIR technique has never been used for investigation of electronic properties of semiconductor photocatalysts, and *in situ* observation of trapped electrons at deeper energy levels was carried out using FT-NIR for the first time. Especially, the energy levels of electron trapping sites for brookite were clarified using FTIR for the first time. The spectral behaviors of TiO_2 powders under N_2+EtOH and under O_2+EtOH were totally different. Moreover, spectral changes during UV irradiation, which is the increment of PA

intensity due to Ti^{3+} generated by electron accumulation, i.e., electron trapping sites, were seen only if the atmosphere in the PA cell was an insert gas containing an electron donor. During UV irradiation, there was a noticeable difference in spectral shape depending on the crystal structure. The results showed that absorption in a low wavenumber region for anatase was larger than that for rutile and brookite. Thus, the results indicate that the energy levels of electron trapping sites greatly depend on the crystal structure and that anatase has shallower energy levels of trapping sites than those of rutile and brookite. Crystal facets and shapes are also thought to affect the trap state energetics because structures of trapping sites are largely determined by the arrangement of constituent atoms (Ti and O atoms) on the exposed crystal face. The electron trapping sites are deep in the order of brookite > rutile > anatase. The FTIR-PAS measurements in the present study offer the FT-NIR technique as a new tool for analysis of electronic properties, for example, energy levels of electron trapping sites and studies on semiconductor materials other than TiO_2 are now in progress.

ASSOCIATED CONTENT

Supporting Information.

Supporting Information is available free of charge on theACS Publications websiteat DOI:10.1021/acs.jpcc.9b02876.

Time-course curves of PA intensity of an aqueous TiO_2 (brookite) suspension, PA intensity of an aqueous TiO_2 (brookite) suspension after addition of methylene blue, FTIR-PAS spectra of carbon black powder, FTIR-PAS spectra of anatase TiO_2 powder (AMT-100) under nitrogen

containing pure water vapor, difference spectra of anatase TiO_2 powders (AMT-100, AMT-600), rutile TiO_2 powders (MT-150A, MT-600B) and brookite TiO_2 powder (PDF)

AUTHOR INFORMATION

Corresponding Author

Naoya Murakami (murakami@life.kyutech.ac.jp)

REFERENCES

(1) Fujishima, A.; Rao, T. N.; Tryk, D. A. Titanium Dioxide Photocatalysis. *J. Photochem. Photobiol., C* **2000**, *1*, 1−21.

(2) Hoffmann, M. R.; Martin, S. T.; Choi, W.; Bahnemann, D. W. Environmental Applications of Semiconductor Photocatalysis. *Chem. Rev.* **1995**, *95*, 69−96.

(3) Amano, F.; Nakata, M.; Yamamoto, A.; Tanaka, T. Effect of Ti^{3+} Ions and Conduction Band Electrons on Photocatalytic and Photoelectrochemical Activity of Rutile Titania for Water Oxidation. *J. Phys. Chem. C* **2016**, *120*, 6467−6474.

(4) Ikeda, S.; Sugiyam, N.; Murakami, S.; Kominami, H.; Kera, Y.; Noguchi, H.; Uosaki, K.; Torimoto, T.; Ohtani, B. Quantitative Analysis of Defective Sites in Titanium(IV) Oxide Photocatalyst Powders. *Phys. Chem. Chem. Phys.* **2003**, *5*, 778−783.

(5) Coronado, J. M.; Maria, A. J.; Conesa, J. C.; Yeung, K. L.; Augugliaro, V.; Soria, J. EPR Study of the Surface Characteristics of Nanostructured TiO_2 under UV Irradiation *Langmuir* **2001**, *17*, 5368−5374.

(6) Berger, T.; Sterrer, M.; Diwald, O.; Knözinger, E.; Panayotov, D.; Thompson, T. L.; Yates, J. T., Jr. Light-Induced Charge Separation in Anatase TiO_2 Particles *J. Phys. Chem. B* **2005**, *109*, 6061−6068.

(7) Kumar, C. P.; Gopal, N. O.; Wang, T. C.; Wong, M.-S.; Ke, S. C. EPR Investigation of TiO_2 Nanoparticles with Temperature-Dependent Properties. *J. Phys. Chem. B* **2006**, *110*, 5223−5229.

(8) Berger, T.; Anta, J. A.; Morales-Flórez, V. Electrons in the Band Gap: Spectroscopic Characterization of Anatase TiO_2 Nanocrystal Electrodes under Fermi Level Control. *J. Phys. Chem. C* **2012**, *116*, 11444−11455.

(9) Kobielusz, M.; Pilarczyk, K.; Świętek, E.; Szaciłowski, K.; Macyk W. Spectroelectrochemical Analysis of TiO_2 Electronic States – Implications for the Photocatalytic Activity of Anatase and Rutile. *Catal. Today* **2018**, *309*, 35–42.

(10) Murakami, N.; Mahaney, O. O. P.; Torimoto, T.; Ohtani, B. Photoacoustic Spectroscopic Analysis of Photoinduced Change in Absorption of Titanium(IV) Oxide Photocatalyst Powders:

A Novel Feasible Technique for Measurement of Defect Density. *Chem. Phys. Lett.* **2006**, *426*, 204−208.

(11) Murakami, N.; Mahaney, O. O. P.; Abe, R.; Torimoto, T.; Ohtani, B. Double-Beam Photoacoustic Spectroscopic Studies on Transient Absorption of Titanium(IV) Oxide Photocatalyst Powders. *J. Phys. Chem. C* **2007**, *111*, 11927−11935.

(12) Nitta, A.; Takashima, M.; Murakami, N.; Takase, M.; Ohtani, B. Reversed Double-Beam Photoacoustic Spectroscopy of Metal-Oxide Powders for Estimation of Their Energy-Resolved Distribution of Electron Traps and Electronic-Band Structure. *Electrochim. Acta* **2018**, *264*, 83−90.

(13) Nitta, A.; Takashima, M.; Takase, M.; Ohtani, B. Identification and Characterization of Titania Photocatalyst Powders Using Their Energy-Resolved Distribution of Electron Traps as a Fingerprint. *Catal. Today* **2019**, *321–322*, 2–8.

(14) Panayotov, D. A.; Yates, J. T., Jr. Spectroscopic Detection of Hydrogen Atom Spillover from Au Nanoparticles Supported on TiO_2: Use of Conduction Band Electrons. *J. Phys. Chem. C* **2007**, *111*, 2959-2964.

(15) Panayotov, D. A.; Burrows, S. P.; Morris, J. R. Infrared Spectroscopic Studies of Conduction Band and Trapped Electrons in UV-Photoexcited, H-Atom n-Doped, and Thermally Reduced TiO_2. *J. Phys. Chem. C* **2012**, *116*, 4535−4544.

(16) Panayotov, D. A.; Burrows, S. P.; Morris, J. R. Photooxidation Mechanism of Methanol on Rutile TiO_2 Nanoparticles. *J. Phys. Chem. C* **2012**, *116*, 6623−6635.

(17) Szczepankiewicz, S. H.; Colussi, A. J.; Hoffmann, M. R. Infrared Spectra of Photoinduced Species on Hydroxylated Titania Surfaces. *J. Phys. Chem. B* **2000**, *104*, 9842-9850.

(18) Litke, A.; Hensen, E. J. M.; Hofmann, J. P. Role of Dissociatively Adsorbed Water on the Formation of Shallow Trapped Electrons in TiO_2 Photocatalysts. *J. Phys. Chem. C* **2017**, *121*, 10153−10162.

(19) Savory, D. M.; Warren, D. S.; McQuillan, A. J. Shallow Electron Trap, Interfacial Water, and Outer-Sphere Adsorbed Oxalate IR Absorptions Correlate during UV Irradiation of Photocatalytic TiO_2 Films in Aqueous Solution. *J. Phys. Chem. C* **2011**, *115*, 902−907.

(20) Savory, D. M.; McQuillan, A. J. Influence of Formate Adsorption and Protons on Shallow Trap Infrared Absorption (STIRA) of Anatase TiO_2 During Photocatalysis. *J. Phys. Chem. C* **2013**, *117*, 23645−23656.

(21) Savory, D. M.; McQuillan, A. J. IR Spectroscopic Behavior of Polaronic Trapped Electrons in TiO_2 under Aqueous Photocatalytic Conditions. *J. Phys. Chem. C* **2014**, *118*, 13680−13692.

(22) Rosencwaig, A.; Gersho, A. Theory of the Photoacoustic Effect with Solids. *J. Appl. Phys.* **1976**, *47*, 64−69.

(23) Ryczkowski, J. Application of Infrared Photoacoustic Spectroscopy in Catalysis. *Catal. Today* **2007**, *124*, 11−20.

(24) Murakami, N.; Shinoda, T Operando Analysis of Electron Accumulation in Titanium(IV) Oxide Particles in an Aqueous Suspension Using a Photoacoustic Spectroscopic Method. *J. Phys. Chem. C* **2019**, *123*, 222–226.

(25) Murakami, N.; Chiyoya, T.; Tsubota, T.; Ohno, T. Switching Redox Site of Photocatalytic Reaction on Titanium(IV) Oxide Particles Modified with Transition-metal Ion Controlled by Irradiation Wavelength. *Appl. Catal. A* **2008**, *348*, 148–152.

(26) Murakami, N.; Shinoda, T. Mid-infrared Absorption of Trapped Electrons in Titanium(IV) Oxide Particles Using a Photoacoustic FTIR Technique. Phys. Chem. Chem. Phys. **2018**, *20*, 24519–24522.

(27) Leytner, S; Hupp, J. T. Evaluation of the energetics of electron trap states at the nanocrystalline titanium dioxide/aqueous solution interface via time-resolved photoacoustic spectroscopy. *Chem. Phys. Lett.* **2000,** *330*, 231–236.

(28) Murakami, N.; Koga, N. In Situ Photoacoustic FTIR Studies on Photocatalytic Oxidation of 2-propanol over Titanium(IV) Oxide. *Catal. Commun.* **2016,** *83*, 1–4.

(29) Liu, Y.; Ying, Y.; Yu, H.; Fu, X. Comparison of the HPLC Method and FT-NIR Analysis for Quantification of Glucose, Fructose, and Sucrose in Intact Apple Fruits. *J. Agric. Food Chem.* **2006**, *54*, 2810-2815.

(30) Lohumi, S.; Lee, S.; Lee, W. H.; Kim, M. S.; Mo, C.; Bae, H.; Cho, B. K. Detection of Starch Adulteration in Onion Powder by FT-NIR and FTIR Spectroscopy. *J. Agric. Food Chem.* **2014**, *62*, 9246–9251.

(31) Zhou, C.; Jiang, W.; Via, B. K.; Fasina, O.; Han, G. Prediction of Mixed Hardwood Lignin and Carbohydrate Content Using ATR-FTIR and FT-NIR. *Carbohydr. Polym.* **2015**, *121*, 336–341.

(32) Mitsui, K.; Inagaki, T.; Tsuchikawa, S. Monitoring of Hydroxyl Groups in Wood during Heat Treatment Using NIR Spectroscopy. *Biomacromolecules* **2008**, *9*, 286–288.

(33) Schilli, C.; Lanzendo1 rfer, M. G.; Müller, A. H. E. Benzyl and Cumyl Dithiocarbamates as Chain Transfer Agents in the RAFT Polymerization of N-Isopropylacrylamide. In Situ FT-NIR and MALDI-TOF MS Investigation. *Macromolecules* **2002**, *35*, 6819-6827.

(34) Suttiwijitpukdee, N.; Sato, H.; Unger, M.; Ozaki, Y. Effects of Hydrogen Bond Intermolecular Interactions on the Crystal Spherulite of Poly(3-hydroxybutyrate) and Cellulose Acetate Butyrate Blends: Studied by FT-IR and FT-NIR Imaging Spectroscopy. *Macromolecules* **2012**, *45*, 2738–2748.

(35) Clarke, F. C.; Jamieson, M. J.; Clark, D. A.; Hammond, S. V.; Jee, R. D.; Moffat, A. C. Chemical Image Fusion. The Synergy of FT-NIR and Raman Mapping Microscopy To Enable a More Complete Visualization of Pharmaceutical Formulations. *Anal. Chem.* **2001**, *73*, 2213-2220.

(36) Czarnecki, M. A.; Morisawa, Y.; Futami, Y.; Ozaki, Y. Advances in Molecular Structure and Interaction Studies Using Near-Infrared Spectroscopy. *Chem. Rev.* **2015**, *115*, 9707–9744.

(37) Schroeder, H.; Buback, J.; Demeshko, S.; Matyjaszewski, K.; Meyer, F.; Buback, M. Speciation Analysis in Iron-Mediated ATRP Studied via FT-Near-IR and Mössbauer Spectroscopy. *Macromolecules* **2015**, *48*, 1981–1990.

(38) Howard, D. L.; Kjaergaard, H. G. Vapor Phase near Infrared Spectroscopy of the Hydrogen Bonded Methanol-Trimethylamine Complex. *J. Phys. Chem. A* **2006**, *110*, 9597-9601.

(39) Grabska, J.; Beć, K. B.; Ishigaki, M.; Huck, C. W.; Ozaki, Y. NIR Spectra Simulations by Anharmonic DFT-Saturated and Unsaturated Long-Chain Fatty Acids. *J. Phys. Chem. B* **2018**, *122*, 6931−6944.

(40) Kadam, S. S.; Windt, E. V. D.; Daudey, P. J.; Kramer, H. J. M. A Comparative Study of ATR-FTIR and FT-NIR Spectroscopy for In-Situ ConcentrationMonitoring during Batch Cooling Crystallization Processes. *Cryst. Growth Des.* **2010**, *10*, 2629–2640.

(41) Murakami, N.; Maruno, H. In Situ Photoacoustic Spectroscopic Analysis on Photocatalytic Decolorization of Methylene Blue over Titanium(IV) Oxide Particles. *RSC Adv.* **2016**, *6*, 65518−65523.

(42) Vequizo, J. J. M.; Matsunaga, H.; Ishiku, T.; Kamimura, S.; Ohno, T.; Yamakata, A. Trapping-Induced Enhancement of Photocatalytic Activity on Brookite TiO_2 Powders: Comparison with Anatase and Rutile TiO_2 Powders. *ACS Catal.* **2017**, *7*, 2644−2651.

(43) Takeuchi, M.; Martra, G.; Coluccia, S.; Anpo, M. Investigations of the Structure of H_2O Clusters Adsorbed on TiO_2 Surfaces by Near-Infrared Absorption Spectroscopy. *J. Phys. Chem. B* **2005**, *109*, 7387-7391.

(44) Takeuchi, M.; Martra, G.; Coluccia, S.; Anpo, M. Verification of the Photoadsorption of H_2O Molecules on TiO_2 Semiconductor Surfaces by Vibrational Absorption Spectroscopy. *J. Phys. Chem. C* **2007**, *111*, 9811-9817.

(45) Schwartz, W. R.; Ciuparu, D.; Pfefferle, L. D. Combustion of Methane over Palladium-Based Catalysts: Catalytic Deactivation and Role of the Support. *J. Phys. Chem. C* **2012**, *116*, 8587−8593.

(46) Guzman, F.; Chuang, S. S. C. Tracing the Reaction Steps Involving Oxygen and IR Observable Species in Ethanol Photocatalytic Oxidation on TiO_2. *J. Am. Chem. Soc.* **2010**, *132*, 1502–1503.

(47) Yamakata, A.; Vequizo, J. J. M.; Matsunaga, H. Distinctive Behavior of Photogenerated Electrons and Holes in Anatase and Rutile TiO_2 Powders. *J. Phys. Chem. C* **2015**, *119*, 24538−24545.

(48) Setvin, M.; Franchini, C.; Hao, X.; Schmid, M.; Janotti, A.; Kaltak, M.; Van de Walle, C. G.; Kresse, G.; Diebold, U. Direct View at Excess Electrons in TiO_2 Rutile and Anatase. *Phys. Rev. Lett.* **2014**, *113*, 086402.

(49) Mattioli, G.; Filippone, F.; Alippi, P.; Bonapasta, A. A. Ab Initio Study of the Electronic States Induced by Oxygen Vacancies in Rutile and Anatase TiO_2. *Phys. Rev. B* **2008**, *78*, 241201.